

## A porphyrin-based probe for simultaneous detection of interface acidity and polarity during lipid phase transition of vesicle

Rini Majumder, Snigdha Roy, Kentaro Okamoto, Satoshi Nagao, Takashi Matsuo, and Partha Pratim Parui

*Langmuir*, **Just Accepted Manuscript** • DOI: 10.1021/acs.langmuir.9b02781 • Publication Date (Web): 10 Dec 2019

Downloaded from [pubs.acs.org](https://pubs.acs.org) on December 11, 2019

### Just Accepted

“Just Accepted” manuscripts have been peer-reviewed and accepted for publication. They are posted online prior to technical editing, formatting for publication and author proofing. The American Chemical Society provides “Just Accepted” as a service to the research community to expedite the dissemination of scientific material as soon as possible after acceptance. “Just Accepted” manuscripts appear in full in PDF format accompanied by an HTML abstract. “Just Accepted” manuscripts have been fully peer reviewed, but should not be considered the official version of record. They are citable by the Digital Object Identifier (DOI®). “Just Accepted” is an optional service offered to authors. Therefore, the “Just Accepted” Web site may not include all articles that will be published in the journal. After a manuscript is technically edited and formatted, it will be removed from the “Just Accepted” Web site and published as an ASAP article. Note that technical editing may introduce minor changes to the manuscript text and/or graphics which could affect content, and all legal disclaimers and ethical guidelines that apply to the journal pertain. ACS cannot be held responsible for errors or consequences arising from the use of information contained in these “Just Accepted” manuscripts.

# A porphyrin-based probe for simultaneous detection of interface acidity and polarity during lipid phase transition of vesicle

Rini Majumder,<sup>†</sup> Snigdha Roy,<sup>†</sup> Kentaro Okamoto,<sup>‡</sup> Satoshi Nagao,<sup>‡</sup> Takashi Matsuo,<sup>\*‡</sup> and Partha Pratim Parui<sup>\*†</sup>

<sup>†</sup>Department of Chemistry, Jadavpur University, Kolkata 700032, India

<sup>‡</sup>Division of Materials Science, Graduate School of Science and Technology, Nara Institute of Science and Technology (NAIST), 8916-5 Takayama-cho, Ikoma, Nara 630-0192, Japan

**ABSTRACT:** Biochemical activities at a membrane interface are affected by local pH/polarity related to membrane lipid properties including lipid dynamics. pH and polarity at the interface are two highly interdependent parameters depending on various locations from the water-exposed outer-surface to the less-polar inner-surface. The optical response of common pH or polarity probes are affected by both the local pH and polarity; therefore, estimation of these values using two separate probes localized at different interface depths can be erroneous. To estimate interface pH and polarity at an identical interface depth, we synthesized a glucose-pendant porphyrin (GPP) molecule for simultaneous pH and polarity detection by a *single* optical probe. pH-induced protonation equilibrium and polarity-dependent  $\pi$ - $\pi$  stacking aggregation for GPP are exploited to measure pH and polarity changes at the 1,2-dimyristoyl-*sn*-glycero-3-phospho-(1-*rac*-glycerol) (DMPG) membrane interface during DMPG phase transition. An NMR study confirmed that GPP is located at the interface Stern layer of DMPG large unilamellar vesicle (LUV). Using UV-vis absorption studies with an adapted analysis protocol, we estimated interface pH, or its deviation from the bulk phase value ( $\Delta$ pH), and the interface polarity simultaneously using the same spectra for sodium dodecyl sulfate (SDS) micelle and DMPG LUV. During temperature dependent gel to liquid-crystalline phase transition of DMPG, there was  $\sim 0.5$  unit increase in  $\Delta$ pH from approximately  $-0.6$  to  $-1.1$ , with a small increase in interface dielectric constant from  $\sim 60$  to  $63$ . A series of spectroscopic data indicate the utility of GPP for evaluation of local pH/polarity change during lipid phase transition of vesicles.

## INTRODUCTION

Cellular events at phospholipid membrane interfaces are associated with the structural dynamics of the membrane, *e.g.*, the lipid phase transition from tightly-packed gel to flexible liquid-crystalline state at room temperature.<sup>1,2</sup> Because the membrane becomes softer in the liquid-crystalline state, endocytosis and exocytosis reactivity are accelerated above the lipid melting temperature.<sup>3,4</sup> Mechanical signal propagation phenomenon such as nerve pulses transmittance is strongly associated with lipids phase transition.<sup>5</sup> However, several other independent investigations have revealed that those membrane biochemical activities are highly sensitive to local pH and polarity surrounding the membrane.<sup>6-8</sup> In this context, we believe that any changes in these physicochemical properties at the membrane interface during lipids phase transition may have profound roles to affect aforementioned membrane reactivity.

Self-assembly occurs at the interface whereby charged/un-charged polar headgroups separates from nonpolar (lipid/surfactant acryl chain) phase and assemble at the polar (aqueous) phases. Thus, pH and polarity at the interface are different from that of the bulk medium. We have recently developed a new interface pH and polarity monitoring method for micelles and vesicles using two *separate* pH and polarity sensitive chromophore probes that interact with the interface.<sup>9,10</sup> However, interface pH and polarity are highly interrelated physicochemical parameters along various interface locations. For example, a decrease of polarity with increasing interface depth towards the hydrophobic phase may decrease interface acidity because of a lack of  $\text{H}_3\text{O}^+$  conduction ability<sup>11</sup>. pH-induced optical changes for a pH probe are frequently affected by solvent polarity<sup>9,10</sup> and *vice versa*. Thus, the precise measurement of pH and polarity using two separate probes localized at different interface depths can be problematic. The simultaneous detection of pH and polarity

at an identical interface depth using a *single* optical probe is proposed here to evaluate either of these two parameters. This is particularly useful for temperature-dependent studies because polarity is intrinsically related to temperature.

Porphyrin derivatives have characteristic absorption bands around 400 nm (Soret band) and 550 nm (Q band). A large extinction coefficient ( $\sim 10^4$ – $10^5 \text{ M}^{-1}\text{cm}^{-1}$ ) at the Soret band is useful as an indicator reagent.<sup>12</sup> Porphyrin derivatives work as pH indicators because of the significant UV-vis spectral changes during protonation at inner nitrogen atoms in the ring. For example, Liu and co-workers reported that tetraphenylporphyrin (TPP)-type compound **1** (Chart 1) works as a pH indicator in the range of pH 4–5, where the electron-donating phenoxy moiety is a key structural factor of pH detection in this range.<sup>13</sup> Furthermore, deprotonated porphyrin compounds (*i.e.* non-protonated state at the inner nitrogen atoms) readily form molecular aggregation states (known as *J*-aggregation or *H*-aggregation) through intermolecular hydrophobic  $\pi$ -stacking under polar environments, whereas the porphyrin compounds exist as a monomer state in non-polar solvents.<sup>14,15</sup> The aggregation behavior is also reflected in the shape of UV-vis spectra of porphyrins. Therefore, the UV-vis spectra of porphyrin derivatives reflect both environmental pH and polarity. According to these characteristics, we expected that TPP-type porphyrins are suitable for simultaneously elucidating the local pH and polarity at a membrane interface.

In this study, we demonstrate the utility of moderately water-soluble glucose-pendant porphyrin GPP (**2**) for monitoring pH and polarity simultaneously at the membrane interface. GPP (**2**) adopts both a neutrally charged (basic form) and cationic forms (acidic form) depending upon the surrounding pH. This assures: 1) binding of GPP (**2**) to the Stern layer of the anionic interface assisted by the cationic charge in the acidic-form porphyrin unit and/or by the dual characteristics of GPP (**2**) with

the *polar* glucose residues and the *nonpolar* basic-form porphyrin unit; and 2) polarity-induced aggregation behavior of GPP (**2**) without affecting the intrinsic protonation property at the porphyrin core. Firstly, we demonstrate the protocol for synchronized evaluation of pH and polarity in homogeneous solvents. Next, we applied this protocol for the simultaneous evaluation of local pH and polarity at the interface of self-assembled sodium dodecyl sulfate (SDS) (**3**) micelles and 1,2-dimyristoyl-*sn*-glycero-3-phospho-(1'-*rac*-glycerol) sodium salt (DMPG) (**4**) vesicles. In addition, we succeeded in the quantitative measurement of interface pH and polarity changes during temperature-induced DMPG phase transition in vesicles.

## EXPERIMENTAL SECTION

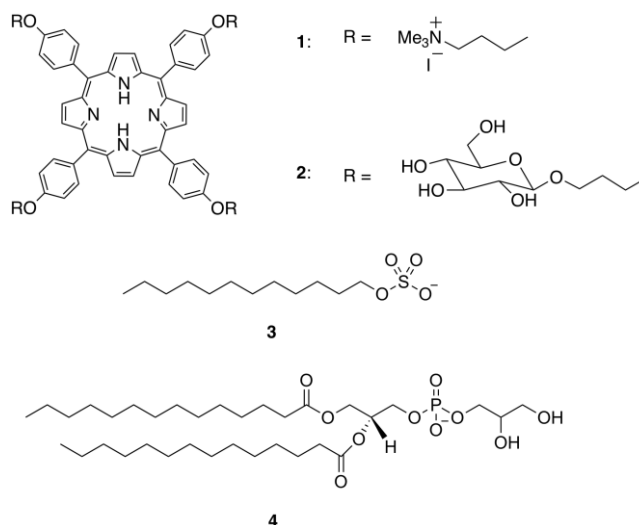
**Materials and Instruments.** Porphyrin **1** was prepared according to a previously reported method.<sup>13</sup> GPP (**2**) and its related intermediate species were synthesized as described in Supporting Information. SDS (**3**) and DMPG (**4**) were purchased from Sigma Aldrich Chemicals (USA) and used without further purification. DMPG large unilamellar vesicle (LUV) was prepared as described below. For preparation of buffers and other analytical measurements, milli-Q Millipore® 18.2 MΩ·cm water was used. Medium pH was measured with a Systronics digital pH meter (Model No. 335). Other chemicals were obtained from conventional vendors. UV-vis spectral changes were followed using a Shimadzu UV-2550 double beam spectrophotometer with a thermostated cell holder. The average particle size for lipid vesicles were evaluated by dynamic light scattering (DLS) measurement with Malvern Instruments, DLS-nano ZS, Zetasizer, Nanoseries. Cryo-transmitted electron microscopy (TEM) experiments were performed with an FEI Tecnai F20 electron microscope equipped with Gatan K2 summit direct detection device. <sup>1</sup>H NMR spectra were collected using a JEOL NM-ECA600 or JNM-ECX400 spectrometers. Differential scanning calorimetry (DSC) measurements were carried out using a Malvern MicroCal VP-DSC calorimeter. Electron ionization mass (EI-MS) measurements were conducted using a JEOL JMS-700 mass spectrophotometer. Matrix-assisted Laser Desorption Ionization mass (MALDI-TOF-MS) spectra were measured using a JEOL JMS-S3000 mass spectrophotometer, where *trans*-2-[3-(4-*tert*-butylphenyl)-2-methyl-2-propenyldene]malononitrile (DCTB) was used as a matrix reagent.

**Preparation of DMPG large unilamellar vesicle (LUV).**<sup>9,16</sup> DMPG was dissolved in 1.0 mL chloroform/methanol (5:1) mixed solvent in 5 mL round bottom flask. The organic solvents were removed rotary evaporator at 35 °C to prepare thin lipid film. Any residual amount of organic solvent was completely removed in vacuo for 3 h. For hydration of prepared thin film, appropriate buffer solution at desired pH was added at 45 °C. The solution was vortexed for 2.0 min for complete dissolution of the lipids to form multi-lamellar vesicles. Seven cycles of freeze-and-thaw were performed between -196 °C and 50 °C to produce giant multilamellar vesicles. To obtain unilamellar vesicles (LUVs) of diameter ~100 nm, the liposome dispersion was extruded 15-times through two stacked polycarbonate membrane filters (Whatman) of 100 nm pore sizes equipped in a Mini-Extruder system (Avanti Polar Lipid, USA). The temperature throughout the LUVs preparation process before and after lipid film hydration was maintained above 30 °C.

**UV-vis absorption studies.** A Quartz cell with 1 cm path-length was used for absorption measurements. All solutions

were filtered through Millipore membrane filter (0.22 μm) before spectroscopic measurements. For temperature variation measurement, the measuring solutions were equilibrated at the particular temperature for 5 min. All measurements were carried out at least three times to check the reproducibility. Different buffer compositions were used to attain a particular medium pH: sodium citrate/sodium phosphate for pH 3.0–5.0; sodium cacodylate-HCl for pH 5.0–6.0; HEPES-NaOH for pH 6.0–7.0. The required amount of GPP (**2**) was added to a buffer solution in the presence and absence of amphiphilic systems, with an addition of either 0.1 M NaOH or 0.1 M HCl to adjust the desired pH, if required. The dielectric constants of mixed solvent medium were determined according to a previous report.<sup>17</sup>

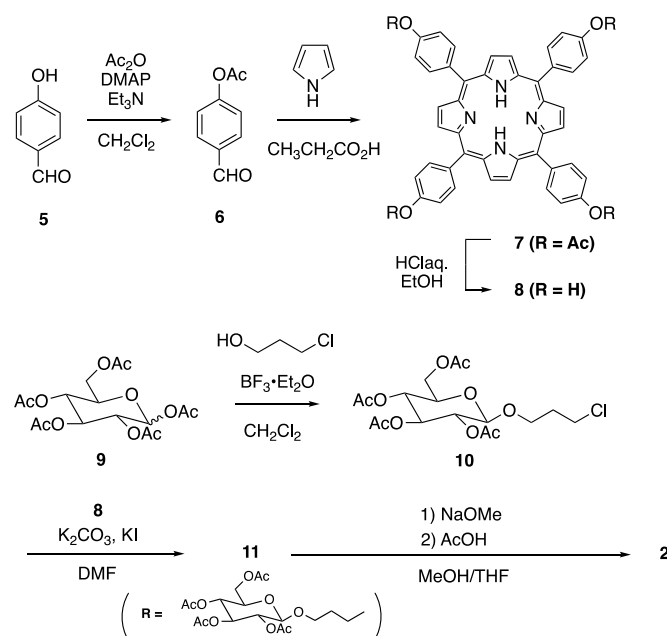
## Chart 1. Chemical structures of TPP-type porphyrins and lipid surfactants.



## RESULTS AND DISCUSSION

**Synthesis of glucose-pendant porphyrin (GPP) 2.** The synthetic route of GPP (**2**) is shown in Scheme 1. The detailed synthetic procedure is described in Supporting Information.

### Scheme 1. Synthetic route of GPP (**2**).



A popular method for the synthesis of compound **8**, a key building block in the synthesis of GPP(**2**), is reflux of a propionic acid solution of 4-hydroxybenzaldehyde (**5**) and pyrrole<sup>13</sup> (the so-called Adler-Longo method<sup>18</sup>). However, the hydrophilic property of **8** (insoluble in CH<sub>2</sub>Cl<sub>2</sub> or CHCl<sub>3</sub>) caused difficulty in separation from turbid and gummy by-products. The low solubility of **5** in CH<sub>2</sub>Cl<sub>2</sub> prevented Lindsay porphyrin synthesis<sup>19</sup> using a Lewis acid catalyst. In contrast, the synthetic route shown in Scheme 1 proved that column purification is not required for obtaining porphyrin **8**. To attach sugar moieties to the periphery of the porphyrin ring, peracetylated glucose with a chloroethyl linker (**10**) was reacted with the phenolic moiety of **8** by Williamson synthesis to yield compound **11**. The in-situ replacement of the chlorine atom in **10** with iodine using potassium iodide (KI) was essential to increase the yield of **11**. Finally, the acetyl groups in **11** were removed under basic conditions to obtain GPP (**2**).

**GPP monomer/aggregate equilibrium: Estimation of polarity.** Firstly, we attempted to evaluate medium polarity (dielectric constant ( $\kappa$ )) by the observation of UV-vis spectral changes in buffer/acetone mixed medium (Figure 1).

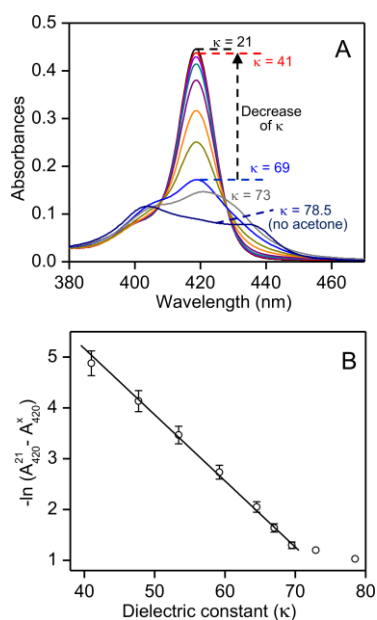


Figure 1. (A) UV-vis absorption spectra of GPP (**2**; 2.5  $\mu$ M) in 10.0 mM sodium citrate/sodium phosphate buffer containing various amounts of acetone% (*w/w*), pH 6.0 at 25  $^{\circ}$ C: red, 60% ( $\kappa = 41.5$ ); violet, 51% ( $\kappa = 47.7$ ); dark cyan, 42% ( $\kappa = 53.4$ ); purple, 33% ( $\kappa = 59.2$ ); orange, 24% ( $\kappa = 64.5$ ); light green, 20% ( $\kappa = 67.0$ ); blue, 16% ( $\kappa = 69.5$ ) and gray, 73% ( $\kappa = 72.9$ ). The spectra in pure buffer ( $\kappa = 78.5$ ) and acetone ( $\kappa = 21.0$ ) medium are shown by dark blue and black, respectively. The change in dielectric constant ( $\kappa$ ) is depicted by the arrow. (B) The negative logarithmic values of intensity difference at 420 nm from pure acetone with  $\kappa \sim 21$  ( $A_{420}^{21}$ ) of other various acetone/buffer mixed mediums with  $\kappa \sim 41.5$ – $69.5$  ( $A_{420}^{\kappa}$ ) are plotted against  $\kappa$ . The values of dielectric constants were quoted from a previous paper.<sup>17</sup>

In buffer (pH > 6.0) at 25  $^{\circ}$ C, GPP (**2**, 2.5  $\mu$ M) exhibited broad absorbances consisting of weak overlapping intensities spreading from  $\sim 400$  to 440 nm (Figure 1A). This spectrum shape is often observed for *H*-type aggregated porphyrins with a small contribution of *J*-type aggregation in aqueous media,<sup>14</sup> where the inner nitrogen atoms in GPP (**2**) are deprotonated.

With an increasing amount of acetone in the buffer, a sharp absorption band around 420 nm appeared with concomitant depletion of those broad bands (Figure 1A). The absorption band around 420 nm is a typical feature of TPP-type porphyrins observed in organic solvents.<sup>20</sup> Although the absorbance changes were not systematic up to 10% (*w/w*) of acetone with dielectric constant ( $\kappa$ )  $\sim 73$  (due to change in aggregation fashion<sup>14, 21</sup> (Figure S1)), the absorbance increased from  $\sim 0.17$  to 0.44 upon the addition of acetone from  $\sim 16\%$  to 60% (*w/w*) with maintaining isosbestic points at  $\sim 407$  and 430 nm (Figure 1A). The quantity of intensity changes at  $\sim 420$  nm were very similar in other organic solvents than acetone (*e.g.* methanol and ethanol, protic solvents) (Figure 1A and S2); suggesting that the observed UV-vis spectral change is interpretable as not specific solvent effect but as polarity effect in the range of solvent  $\kappa$  from approximately 41 to 69. The series of observed spectral changes indicate that the deprotonated GPP undergoes an interconversion equilibrium between the aggregated form (denoted as  $d_A$ -GPP) and the monomer form ( $d_M$ -GPP), where “d”, “A” and “M” stand for “deprotonated”, “aggregated”, and “monomer”, respectively.

In contrast to GPP (**2**), porphyrin **1** showed a distinct absorption band at  $\sim 420$  nm in aqueous medium with comparable intensity to that observed for GPP (**2**) in the presence of organic solvents (Figure S3). The absorption pattern and intensity increased a little (< 10%) in the presence of methanol or acetone in buffer at pH 7.0. These results demonstrate that the UV-vis spectra of porphyrin **1** are less sensitive on solvent polarity compared to GPP (**2**). The spectral changes indicate that porphyrin **1** predominantly exists as a monomer form in the buffer solution because of cationic ammonium moieties. Therefore, GPP (**2**) is superior to **1** as a polarity indicator.

The  $d_A$ -GPP to  $d_M$ -GPP interconversion equilibrium was found to depend on medium temperature as well. For the mixed medium containing different acetone ratios (24–50%) in buffer, the intensity at  $\sim 420$  nm for GPP (**2**; 2.5  $\mu$ M) increased gradually with rising temperature from 20  $^{\circ}$ C to 45  $^{\circ}$ C (Figure S4). Both the increase in temperature and in acetone ratio displayed a similar decrease in solvent  $\kappa$   $\sim 5.5$ – $6.0$  units (Figure 1A and S4A).<sup>17</sup> Namely, the temperature-induced absorbance change at  $\sim 420$  nm is regarded as the temperature affected change in medium  $\kappa$ .<sup>17</sup> Therefore,  $\kappa$  of GPP (**2**) localized environment can be estimated by monitoring  $d_A$ -GPP to  $d_M$ -GPP interconversion based on the absorbance change at  $\sim 420$  nm. Accordingly, we empirically correlate the absorbance change at  $\sim 420$  nm and medium  $\kappa$ . The negative logarithmic value for the amount of intensity decrease at  $\sim 420$  nm from the saturated intensity at  $\kappa < 35$  under complete conversion to  $d_M$ -GPP exhibited a linear correlation with solvent  $\kappa$  in the range from  $\kappa \sim 40$  to 70 (Figure 1B), and thus  $\kappa$  can be estimated by using the eq.(1):

$$-\log(A_{420}^{21} - A_{420}^{\kappa}) = -0.13 \times \kappa + 10.3 \quad (40 \leq \kappa \leq 70) \quad (1)$$

where  $A_{420}^{21}$  and  $A_{420}^{\kappa}$  represent the absorbance value at  $\sim 420$  nm in acetone medium ( $\kappa = 21$ ) and the observed absorbance for a solution at unknown polarity (*i.e.* an observation target), respectively. The intercept and slope values are represented by 10.3 and  $-0.13$ , respectively.

**GPP acid/base equilibrium: Estimation of pH.** Next, we attempted to develop the protocol for evaluation of pH at various

polarity conditions based on the UV-vis spectra of GPP (2). In pH-dependent UV-vis absorption studies for GPP (2.5  $\mu\text{M}$ ) in a buffer solution, a new absorption band at  $\sim 446$  nm appeared with the decrease in the broad band of  $d_A$ -GPP on decreasing pH from 5.5 (Figure 2A). The spectral change is due to the protonation at inner nitrogen atoms in the porphyrin ring. The absorbance increase saturated at pH below 3.5, suggesting a complete protonation at inner nitrogen atoms in GPP.<sup>12</sup> A much sharper Soret band of the protonated GPP compared to  $d_A$ -GPP (Figure 2A) indicates that the protonated GPP exists in the monomeric state. Namely, the protonated GPP is denoted as “ $p_M$ -GPP”, where “p” stands for “protonated” form. In the presence of buffer containing different acetone ratios, the single isosbestic point in the pH-dependent spectral changes indicate the apparent one-step interconversion of two deprotonated forms ( $d_A$ -GPP and  $d_M$ -GPP) (at high pH,  $\lambda_{\text{abs}} \sim 420$  nm) into protonated  $p_M$ -GPP (at low pH,  $\lambda_{\text{abs}} \sim 450$  nm and 685 nm) (Figure 2B and S5). The whole porphyrin interconversion reflected in Figures 2A and 2B are summarized in Scheme 2.

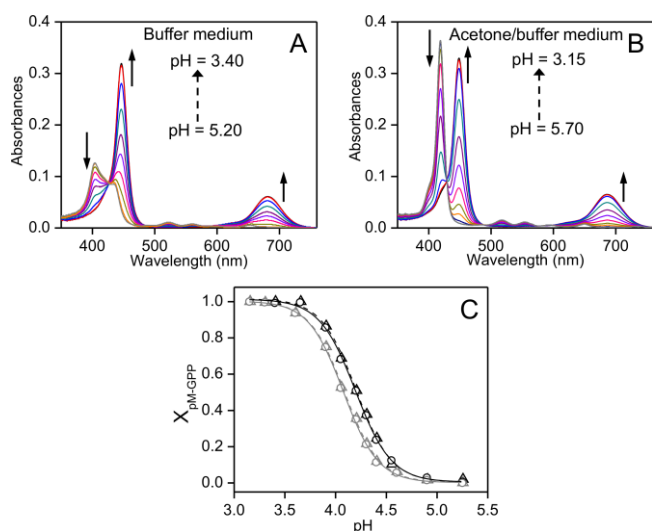
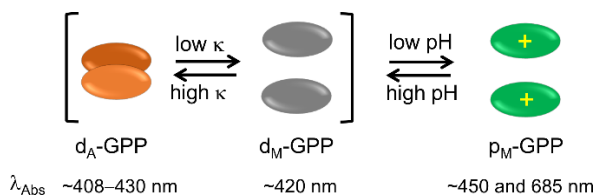


Figure 2. pH-dependent UV-vis analyses of GPP (2; 2.5  $\mu\text{M}$ ) at 25  $^{\circ}\text{C}$ : (A) Spectral changes observed in 10 mM sodium citrate/sodium phosphate buffer, pH 3.40, 3.70, 3.90, 4.05, 4.20, 4.30, 4.40, 4.55, 4.90, and 5.20; (B) Spectral changes observed in the buffer containing 31% (w/w) acetone, pH 3.15, 3.40, 3.60, 3.90, 4.05, 4.20, 4.30, 4.40, 4.60, 4.90, 5.25, and 5.7. The change in intensities with decreasing pH are shown in arrows. (C)  $p_M$ -GPP mole-ratio ( $X_{pM-GPP}$ ) analyzed from the intensity at  $\sim 450$  nm (circle, solid lines) and  $\sim 685$  nm (triangle, broken lines) are plotted against pH: black, 10 mM sodium citrate/sodium phosphate buffer; gray, 31% (w/w) acetone containing buffer.

**Scheme 2. pH and dielectric constant ( $\kappa$ ) dependent interconversion equilibrium among aggregated-deprotonated ( $d_A$ -GPP), monomeric-deprotonated ( $d_M$ -GPP) and monomeric-protonated ( $p_M$ -GPP) forms of GPP.**



Electrostatic repulsion between positively-charged porphyrins with protonated inner nitrogen atoms prevents the hydrophobic  $\pi$ -stacking interaction resulting in the existence of the monomeric state, even in pure aqueous buffer. By following a similar trend, another relatively weak absorption intensity at  $\sim 685$  nm also increased systematically with decreasing pH, suggesting that both intensities at  $\sim 446$  and  $\sim 685$  nm are associated with the  $p_M$ -GPP form (Figure 2A). Therefore, the equilibrium mole-ratio of  $p_M$ -GPP ( $X_{pM-GPP}$ ) can be determined by analyzing the absorption intensities at  $\sim 446$  nm and  $\sim 685$  nm as follows:

$$X_{pM-GPP} = (A_{\lambda}^{\text{pH}} - A_{\lambda}^{6.0}) / (A_{\lambda}^{3.5} - A_{\lambda}^{6.0}) \quad (2)$$

where  $A_{\lambda}^{\text{pH}}$  and  $A_{\lambda}^{3.5}$  represent the pH-dependent absorbance and the saturated intensities below pH 3.5 at wavelength ( $\lambda$ )  $\sim 446$  or  $\sim 685$  nm, respectively.  $A_{\lambda}^{6.0}$  denotes the absorption intensity at  $\sim 446$  nm or  $\sim 685$  nm when GPP exists as deprotonated state ( $d_M$ -GPP and/or  $d_A$ -GPP) at pH above 6.0. The mole-ratios of  $p_M$ -GPP ( $X_{pM-GPP}$ ) were plotted with pH (Figure 2C), and the acid/base  $pK_a$  for GPP was estimated to be  $\sim 4.2$  by fitting data points with a sigmoidal-Boltzmann equation (the data of first row in Table S1). The unknown pH of an aqueous medium can be estimated from the pH vs.  $p_M$ -GPP mole-ratio calibration curve.

The pH vs.  $p_M$ -GPP mole-ratio calibration curve in acetone/buffer solutions shifted to the direction of lower pH compared to the pure buffer solution (*cf.* black and gray lines in Figure 2C). The deviation reflects the polarity effect on the protonation/deprotonation equilibrium. This indicates that the contributions of solvent  $\kappa$  and pH should be separated in the observed UV-vis spectral changes in order to develop the protocol to estimate pH under variable polarity conditions.

Accordingly, we performed the pH-metric titration of GPP under various polarity conditions to monitor the interconversion from  $d_A$ -GPP and/or  $d_M$ -GPP to  $p_M$ -GPP (Figures S5 (A–E)). Similar to the spectral change observed in buffer solutions, a sharp band around  $\sim 450$  nm for  $p_M$ -GPP form gradually appeared with decreasing pH from 6.0 to 2.5. The apparent acid/base  $pK_a$  decreased from  $\sim 4.10$  to 3.35 with decreasing solvent  $\kappa$  from  $\sim 62.0$  to  $\sim 42.0$  at 25  $^{\circ}\text{C}$  (Table S1, Figure S5). The lack in solvation of cationic  $p_M$ -GPP at low  $\kappa$  results in the decrease in apparent  $pK_a$ . Since the magnitude of  $A_{\lambda}^{6.0}$  (in eq. 2) is independent of medium polarity ( $\kappa \leq 70$ ), the pH dependent  $p_M$ -GPP/GPP ratio ( $X_{pM-GPP}$ ) can be estimated independently without knowing the  $\kappa$  of mixed solvents.

For the acetone/buffer mixed medium, temperature dependent  $pK_a$  values are estimated and listed in Table S1. Interestingly, a certain decrease in solvent  $\kappa$  by either an increase in acetone ratio or increase in temperature in the buffer/acetone mixed medium exhibited a similar extent in acid/base  $pK_a$  shift (Table S1, Figures S5 and S6). These results suggest that the temperature-dependent  $pK_a$  shift for GPP is mostly associated with the variation of solvent  $\kappa$  (Figures S5 and S6). Therefore, maintaining an identical temperature condition of the measuring and calibrating solutions is a prerequisite to determine the GPP environmental pH by utilizing pH-metric titration curves.

**Simultaneous estimation of pH and polarity in homogeneous solutions.** Under complete protonation of GPP, the identical absorption intensity at various solvent  $\kappa$  (Figure 2 for buffer solutions, Figure S5 for acetone-containing buffer solutions,

and in Figure S6 for solutions at different temperatures) indicates molar extinction coefficients ( $\epsilon$ ) at all wavelengths does not depend upon medium  $\kappa$ . However, when GPP becomes partially protonated, the intensity change at  $\sim 420$  nm is to be affected not only by the  $\kappa$ -induced change in  $d_A$ -GPP to  $d_M$ -GPP ratio for the deprotonated GPP, but also their protonation to form  $p_M$ -GPP. By evaluating  $X_{pM-GPP}$  from eq. (2), the intensity due to  $p_M$ -GPP form at  $\sim 420$  nm is calculated as  $A_{420}^p \times X_{pM-GPP}$ , where  $A_{420}^p$  denotes the intensity for the fully protonated GPP ( $X_{pM-GPP} = 1$ ). Therefore, the actual intensity of deprotonated GPP ( $d_A$ -GPP and/or  $d_M$ -GPP) at  $\sim 420$  nm can be obtained by subtracting  $A_{420}^p \times X_{pM-GPP}$  from the observed intensity ( $A_{420}^{obs}$ ). Furthermore,  $(A_{420}^{obs} - A_{420}^p \times X_{pM-GPP})$  was normalized by dividing it with the mole-ratio of deprotonated GPP ( $1 - X_{pM-GPP}$ ) to use eq. (1) for the estimation of  $\kappa$ :

$$A_{420}^N = A_{420}^x = (A_{420}^{obs} - A_{420}^p \times X_{pM-GPP}) / (1 - X_{pM-GPP}) \quad (3)$$

$$-\log(A_{420}^{21} - A_{420}^x)$$

$$= -\log[A_{420}^{21} - (A_{420}^{obs} - A_{420}^p \times X_{pM-GPP}) / (1 - X_{pM-GPP})]$$

$$= -0.13 \times \kappa + 10.3 \quad (4)$$

Using eq. 4, an unknown  $\kappa$  can be estimated by evaluating  $X_{pM-GPP}$  and  $A_{420}^N$  from the intensities at  $\sim 450$  or  $685$  nm and  $420$  nm, respectively. Notably, the more general eq. 4 than eq. 1 can be used to estimate  $\kappa$  under the conditions of various extent of GPP protonation in a wide range of bulk pHs. Once the medium  $\kappa$  is known, pH of the medium can also be simultaneously estimated from the same absorption spectrum by correlating  $X_{pM-GPP}$  with the pH-metric calibration curve obtained under same medium  $\kappa$ .

A series of test of the above procedure above demonstrated that GPP (2) is a highly effective for simultaneous detection of environmental pH and  $\kappa$  using a single absorption spectrum.

**Interaction of GPP with self-assembly interfaces.** Encouraged by the proved utility of GPP (2) for simultaneous determination of the local polarity and pH around the molecule, we investigated the availability of GPP (2) for probing the local environment at the interface of lipid emulsions. Firstly, we attempted to elucidate interaction fashions between GPP (2) and DMPG LUV by  $^1H$  NMR spectroscopy. The full 1D  $^1H$  NMR spectrum of the mixture of GPP (2) and DMPG LUV observed at  $40^\circ C$  is shown in Figure 3A. Figure 3B shows the temperature dependency on 1D  $^1H$  NMR spectrum in the range from 7.0 to 10.0 ppm. The diameter of DMPG LUV at  $\sim 100$  nm was controlled by the lipid extrusion (see Experimental Section) and the size distribution and morphology were further confirmed by DLS and cryo-TEM analysis, respectively (Figures S7 and S8).

The signals at 7.5 ppm, 8.3 ppm, and 9.1 ppm are assigned as protons of *m*-phenyl, *o*-phenyl and porphyrin  $\beta$ -positions, respectively (supporting information). The signal broadening is wholly due to the existence of LUV macromolecular substance. At lower temperatures, each signal tends to split into two peaks (Figure 3B). The splitting occurs around  $25$ – $30^\circ C$ , which is close to the phase transition temperature of DMPG LUV (*vide infra*).<sup>22, 23</sup> Consequently, this finding indicates that GPP (2) interacts with DMPG LUV. The signal splitting at low temperatures is caused by the decrease in exchange rate between several interaction fashions. We also collected the NOESY spectrum of the mixture of GPP (2) and DMPG LUV at  $40^\circ C$  in order to address the location of GPP (2) in DMPG LUV (Figure 3C).

The protons signals at 7.5 ppm, 8.3 ppm and 9.1 ppm of 2 displayed correlation signals with proton peaks at 4.1 ppm and 4.5 ppm, corresponding to the protons at the head moiety of DMPG. Similar cross peaks were also observed in the measurement at  $20^\circ C$  (Figure S9). The results of 2D NMR spectral analysis strongly indicate that GPP (2) locates on the interface Stern layer of DMPG LUV regardless of temperature change. Therefore, GPP (2) is suitable to measure pH and polarity at a similar Stern layer location for DMPG LUV during the temperature-induced lipid phase transition.

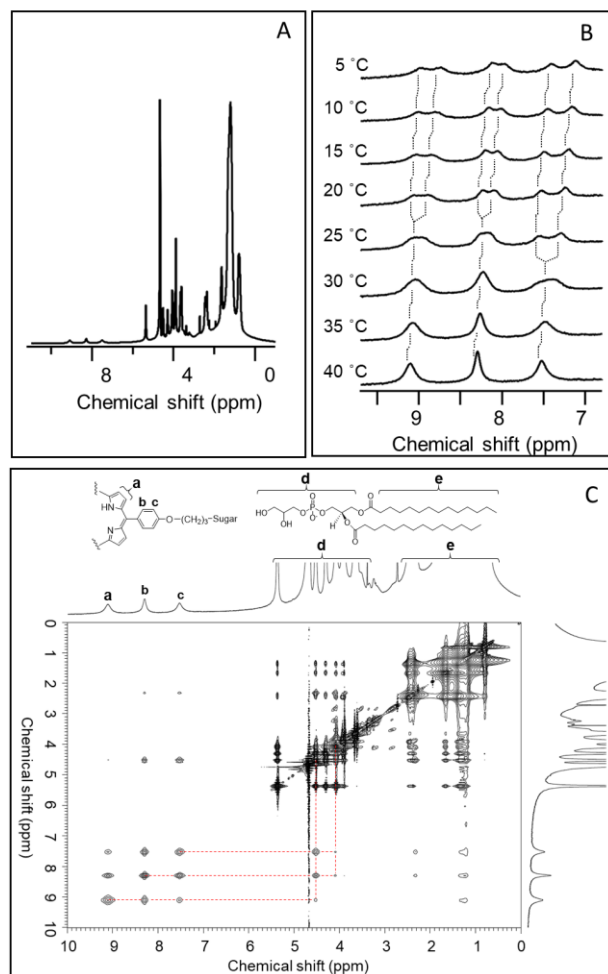


Figure 3. 600 MHz- $^1H$  NMR spectroscopic analysis for the mixture of GPP(2) and DMPG LUV; (A) Whole 1D NMR spectrum at  $40^\circ C$ ; (B) 1D NMR spectra at various temperatures in the range from 7.0 ppm to 10.0 ppm; (C) NOESY spectrum at  $40^\circ C$ ; Conditions: [2] = 1 mM, [DMPG LUV ( $d \sim 100$  nm)] = 8 mM in  $D_2O$  containing  $DMSO-d_6$  (5% v/v)) The dotted lines marked in Figure 3(B) indicate the signal shifts of the protons during change in temperature. Red broken lines in Figure 3(C) indicate the correlations between the protons in GPP (2) and those in the head moiety of DMPG.

Next, we measured UV-vis spectra of GPP in the presence of amphiphilic systems. The absorbances at  $\sim 450$  nm or  $\sim 685$  nm for GPP (2.5  $\mu M$ ) in 10 mM citrate/phosphate buffer (pH 4.2) increased gradually with increasing concentration of SDS micelles or DMPG LUV (Figure S10). This is indicative of the interaction between GPP and the interface of those self-assemblies. The increase in absorbances shown in Figure S10 is very similar to the spectral change observed for the pH titration in a buffer solution (Figure 2A), suggesting GPP in the amphiphilic

systems undergoes the acid/base equilibrium to generate  $p_M$ -GPP form. No significant changes in LUV morphology is confirmed by the observation of almost identical distribution in DMPG LUV diameter (Figure S7). The intensities saturated in the presence of 8 mM SDS or 1.1 mM DMPG, and the intensity saturation justifies that all the GPP molecules interacted with the interface. The red-shift of absorption band from  $\sim 446$  to 450 nm for  $p_M$ -GPP form in the self-assembled system suggests GPP interacted with the self-assembly interface with  $\kappa$  lower than the bulk phase. Therefore, we performed further measurement under these micelle or LUV-interacting intensity saturation conditions to monitor  $d_A$ -GPP and/or  $d_M$ -GPP to  $p_M$ -GPP interconversion for GPP at the self-assembly interfaces.

**Simultaneous estimation of pH and polarity at the self-assembly interfaces.** pH-metric titrations for GPP(2) were performed with an interaction saturated high concentration of DMPG LUV (lipid, 1.1 mM, Figure 4A) and SDS micelles (8 mM, Figure S11B) at 25 °C. As described above, the extinction coefficient of  $p_M$ -GPP form does not depend on  $\kappa$ . The pH-dependent equilibrium  $p_M$ -GPP mole-ratio ( $X_{p_M-GPP}$ ) at the DMPG LUV interface was estimated by monitoring absorption intensity at  $\sim 450$  nm or  $\sim 685$  nm at the full interaction of GPP with self-assembled systems according to eq. (2). On the other hand, for the determination of  $X_{p_M-GPP}$  value at the SDS micelle interface, only absorbance change at  $\sim 685$  nm can be used for the analysis. The higher energy absorption band around 450 nm tended to gradually blue-shift with decreasing pH from 5.3 to 4.3 and overlapped considerably with that of  $d_A$ -GPP and/or  $d_M$ -GPP (Figures S11B). When using  $X_{p_M-GPP}$  under different bulk pH conditions, the interface  $\kappa$  was estimated by calculating the corresponding  $A_{419}^N$  from the observed intensity at  $\sim 420$  nm according to eq. 3 and 4. The interface  $\kappa$  were determined to be similar at  $\sim 61.5$  and 60.5 for SDS micelle and DMPG LUV, respectively, at 25 °C using eqs. 3 and 4 (Table 1).

**Table 1 Temperature- and bulk pH- dependent pH deviation from the bulk to the interface ( $\Delta$ pH) and interface dielectric constant ( $\kappa(i)$ ) for SDS micelle and DMPG LUV**

	T (°C)	Bulk pH	Interface $\kappa$	$\Delta$ pH
SDS micelle	20	4.3–5.3	$63.0 \pm 0.2$	$-0.72 \pm 0.03$
	25	4.3–5.3	$61.5 \pm 0.2$	$-0.70 \pm 0.03$
	35	4.2–5.2	$59.4 \pm 0.2$	$-0.69 \pm 0.03$
	40	4.1–5.1	$57.6 \pm 0.2$	$-0.67 \pm 0.03$
DMPG LUV	20	4.5	$61.6 \pm 0.4$	$-0.62 \pm 0.03$
		4.9–5.3	$61.5 \pm 0.2$	$-0.62 \pm 0.03$
	25	4.5	$60.6 \pm 0.4$	$-0.67 \pm 0.03$
		4.9–5.3	$60.3 \pm 0.2$	$-0.67 \pm 0.03$
	30	4.5	$59.6 \pm 0.4$	$-0.85 \pm 0.03$
		4.9–5.3	$61.9 \pm 0.2$	$-1.01 \pm 0.03$
	35	4.5	$62.1 \pm 0.4$	$-1.05 \pm 0.03$
		4.9–5.6	$63.0 \pm 0.2$	$-1.09 \pm 0.03$
	40	4.5	$62.6 \pm 0.4$	$-1.10 \pm 0.03$
		4.9–5.6	$61.4 \pm 0.2$	$-1.11 \pm 0.03$

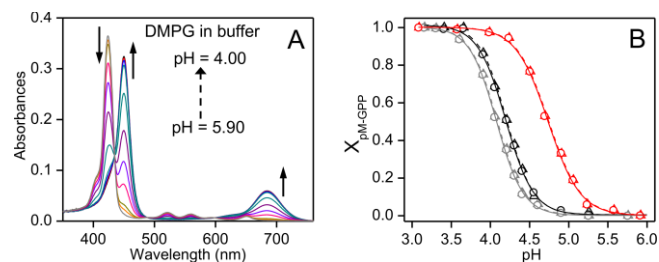


Figure 4. pH-dependent UV-vis analysis of GPP (2; 2.5  $\mu$ M) at 25 °C in 10 mM sodium citrate/sodium phosphate buffer containing DMPG LUV (lipid, 1.1 mM); (A) Spectra measured at pH 4.0, 4.25, 4.50, 4.70, 4.90, 5.05, 5.25, 5.55, 5.90. The change in intensities with decreasing pH are shown in arrows; (B)  $p_M$ -GPP mole-ratio ( $X_{p_M-GPP}$ ) analyzed from the intensity at  $\sim 450$  nm (circle, solid lines) and  $\sim 685$  nm (triangle, broken lines) are plotted against bulk pH (red). The plots for pure buffer solutions (black) and buffer containing 31% (w/w) acetone (gray) in Figure 2 are shown for comparison.

The interface pH can be evaluated by monitoring the bulk pH-dependent  $p_M$ -GPP mole-ratio between the interface and the bulk. The increase in the amount of  $p_M$ -GPP mole-ratios observed in self-assembled systems indicate that the interfaces of these self-assemblies provide more acidic environments than the bulk phase does (DMPG LUV: Figure 4; SDS: Figure S11B). For quantitative measurement of pH at the interface, the  $p_M$ -GPP mole-ratio in the absence and presence of interaction saturated high concentration of SDS or DMPG LUV are compared with that of bulk pH (Figures 4B and S11E). The apparent pH shift between the interface and the bulk pH ( $\Delta$ ) can be estimated from the difference in  $p_M$ -GPP ratio between the interface and the bulk at 25 °C, where  $\Delta$  should be negative because the interface is more acidic compared to the bulk. Irrespective of a different bulk pH, the  $\Delta$  value was estimated to be approximately  $-0.54$  and  $-0.59$  for DMPG LUV and SDS micelles, respectively (Figures 4 and S11). Because the pH-induced interconversion between  $p_M$ -GPP and  $d_A$ -GPP and/or  $d_M$ -GPP is also affected by medium  $\kappa$ ,  $\Delta$  can also be affected by the difference in  $\kappa$  between the interface and the bulk. The polarity contribution ( $\delta$ ) to  $\Delta$  is estimated by the apparent pH shift caused by the difference in  $\kappa$  between the interface and the bulk. The pH deviation ( $\Delta$ pH) from the bulk to the interface pH ( $pH_{inf}$ ), and subsequently  $pH_{inf}$  are obtained from the bulk pH ( $pH_{bulk}$ ),  $\Delta$ , and  $\delta$ :

$$\Delta pH = \Delta - \delta \quad (5)$$

$$pH_{inf} = pH_{bulk} + \Delta - \delta \quad (6)$$

$\Delta$  is the function of combined interface pH and  $\kappa$ , whereas  $\delta$  is related to interface  $\kappa$ . Conventionally, two separate pH and polarity responsive probe molecules are used to evaluate  $\Delta$  and  $\delta$ , respectively.<sup>9, 10</sup> However, the change in the locations of these pH and polarity probes at various interface depths makes the determination of  $\delta$  erroneous because the interface polarity can decrease drastically with increasing interface depth from the water-exposed outer-surface. In contrast, the simultaneous estimation of  $\Delta$  and  $\delta$  parameters using a *single* GPP probe at an *identical* interface depth not only enables us to compute the correct value of  $\delta$  for measuring interface pH, but also provides simultaneous values of interface pH and  $\kappa$ .

The value of  $\kappa$  in acetone/buffer mixed solution was adjusted same as the interface  $\kappa$  for SDS micelles and DMPG LUV at 25 °C (Table 1), and  $\delta$  was found to be  $\sim 0.11$  for SDS micelles and  $\sim 0.13$  DMPG LUV, respectively, under different

pH conditions at 25 °C (Figure S5 (B, F and G)). With the variation of bulk pH, the estimated pH deviation from the bulk to the interface ( $\Delta\text{pH}$ ) for SDS micelles and DMPG LUV were found to be similar  $\sim 0.70$  and  $\sim 0.67$ , respectively, at 25 °C (Table 1, Figures 4B, and S5 (B, F and G)). For anionic self-assemblies, the negatively charged headgroup at the interface may involve attractive electrostatic interaction with  $\text{H}^+$ , but it repels  $\text{OH}^-$ . In comparison to the bulk phase,  $[\text{H}^+]$  and  $[\text{OH}^-]$  may increase and decrease, respectively, at the interface. However,  $[\text{H}^+]$  and  $[\text{OH}^-]$  remain unchanged in the bulk owing to the larger volume of the bulk phase than the interface. Therefore, higher  $[\text{H}^+]$  at the anionic SDS micelle or DMPG LUV interface than the corresponding bulk phase makes the interface more acidic compared to the bulk pH.

**Temperature effect on SDS micelle interface pH and polarity.** The general temperature effect on interface pH and  $\kappa$  were examined for SDS micelle. Upon increasing the temperature from 20 °C to 40 °C, the acid/base  $\text{p}K_a$  at the SDS micelle interface decreased from  $\sim 4.8$  to 4.6 (Table S2 and Figure S11). At first, the dependency of interface  $\kappa$  on temperature was estimated by analyzing the intensity contribution of  $d_M\text{-GPP}$  from absorption spectra under various pH conditions according to eq. 1 (for complete deprotonation of GPP,  $\text{pH} > 7.0$ ) or eq. 4 (for a mixture of protonated and deprotonated GPP,  $\text{pH} < 7.0$ ). Irrespective of different bulk pH, the observed intensity (for  $\text{pH} \geq 7.0$ ) or normalized intensity ( $A_{420}^N$  for  $\text{pH} < 7.0$ ) at 420 nm increased from  $\sim 0.34$  to 0.39 with an increase of temperature from 25 °C to 40 °C (Figure S11), which corresponds to a decrease of interface  $\kappa$  from  $\sim 61.5$  to 57.6 (Table 1 and Figure S5). Interestingly, the identical decrease of  $\kappa$  from 25 °C to 40 °C was observed for 31% acetone-containing buffer medium (Table S1, Figures S4 and S5), suggesting that the typical temperature vs.  $\kappa$  correlations are also maintained at the SDS micelles interface. In addition, a similar amount of  $\text{p}K_a$  decrease  $\sim 0.2$  for GPP between SDS micelle and acetone/buffer medium with  $\kappa$  similar to that of the SDS interface was detected by the increase of temperature from 25 °C to 40 °C (Tables S1 and S2, Figures S6 and S11). The results shows that the interface pH for SDS micelle remains unchanged and the acid/base  $\text{p}K_a$  change for GPP is caused by the temperature induced variation of interface  $\kappa$ .

**Interface pH/polarity changes during temperature induced phase transition for DMPG LUV.** The gel to liquid-crystalline phase transitions process of lipids in LUV membrane is not only affected by temperature, but also dependent on environmental pH conditions.<sup>24</sup> DMPG is known to exhibit weakly energetic pre-transitions peaks at low temperatures ( $\sim 11\text{--}15$  °C) and highly cooperative strongly energetic gel to liquid-crystalline phase transitions ( $\sim 23\text{--}25$  °C).<sup>25</sup> The phase transition temperatures ( $T_m$ ) of DMPG in its LUV were measured by differential scanning calorimetry (DSC) in 10 mM citrate/phosphate buffer solution at various pH 4.5–5.5 (Figure 5). The weak pre-transition peak at  $\sim 16$  and 21 °C were observed at pH 5.5 and 5.0, respectively, although no such peak appeared at pH 4.5. However, the main phase transition temperature  $T_m$ ,<sup>26</sup> was found to increase from 28.0 to 32.3 °C by decreasing pH from 4.9 to 4.5, whereas  $T_m$  increased to a relatively lower extent from 26.6 to 28.0 °C with increasing pH to 5.5.

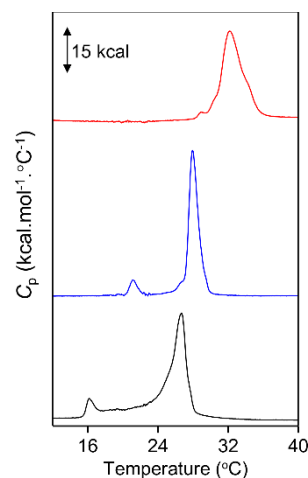


Figure 5. Differential scanning calorimetry (DSC) thermograms of DMPG LUV (lipids, 1 mM) in 10 mM citrate-phosphate buffer, pH 4.5 (red), pH 4.9 (blue), and pH 5.5 (black).

Temperature- and pH-dependent acid/base equilibrium for GPP (2.5  $\mu\text{M}$ ) were monitored at the DMPG LUV interface to monitor the effect of phase transition from DMPG gel state to its liquid-crystalline state on the interface pH and  $\kappa$  (Figure S12). In contrast to SDS micelles, an increase in absorption intensity at  $\sim 450$  nm and  $\sim 685$  nm was observed for DMPG LUV by increasing temperature from 20 °C to 40 °C (Figure 6 and S12) under a different, but constant pH. However, major increases in absorption intensity at  $\sim 450$  nm from  $\sim 0.12$  to 0.21 and at  $\sim 685$  nm (from  $\sim 0.02$  to 0.04) were detected between 25 °C and 35 °C at bulk pH 4.9. No further intensity increase was observed at above 35 °C (Figure 6 and Table 1). Under a decreased bulk pH condition of 4.5, a major increase in intensity was noticed at above 30 °C up to 40 °C (Figure 6B). The increase in  $T_m$  for DMPG LUV from 28.0 °C to 32.3 °C with decreasing pH from 4.9 to 4.5 also clearly correlates with the increasing temperature required to obtain the major increase in  $p_M\text{-GPP}$  mole-ratio from 4.9 to 4.5 (Figure 6). The temperature induced increase in  $p_M\text{-GPP}$  mole-ratio indicating an increase in interface acidity can be correlated with the phase transitions process of DMPG gel state to liquid-crystalline state (Figure 6 and Table 1).

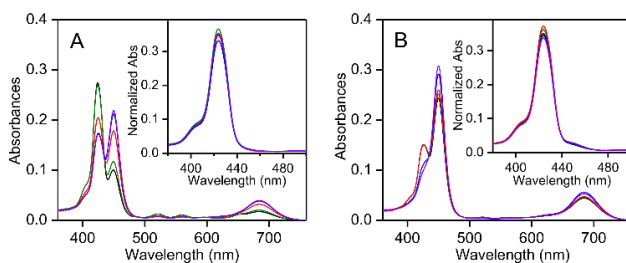


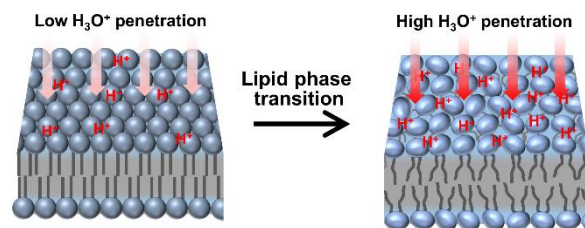
Figure 6. Temperature dependent UV-vis absorption spectra of GPP (2; 2.5  $\mu\text{M}$ ) and (inset) corresponding normalized absorption spectrum in 10 mM sodium citrate/sodium phosphate buffer containing DMPG LUV (1.1 mM) at (A) pH 4.9 and (B) pH 4.5: black, 20 °C; green, 25 °C; red, 30 °C; blue, 35 °C and violet, 40 °C. Each spectrum in inset is normalized according to the similar procedure to obtain normalized intensity ( $A_{420}^N$ ) using eq. (3).

According to our analysis protocol, we first estimated interface  $\kappa$  by normalizing each spectrum in Figure 6 and S12. For example, normalized spectra at pH 4.9 and 4.5 according to eq.

3 are represented in inset of Figure 6. Interface  $\kappa$  for DMPG LUV at different temperatures and pH values were determined from the value of normalized intensity ( $A_{420}^N$ ) using eq. 4 (Figures 6, S12 and Table 1). When DMPG involves a phase transition process from  $\sim 25$  °C to 35 °C at pH 4.9 and  $\sim 30$  °C to 40 °C at pH 4.5, the interface  $\kappa$  increased from 60.3 to 63.0 and 59.6 to 62.6, respectively (Figures 5, 6 and Table 1). For other temperatures when DMPG did not involve a phase transition significantly according to DSC measurements (Figure 5), a decrease in interface  $\kappa$  with increasing temperature was also observed in similar to SDS micelles (Figure S11, and Table 1 and S1). Since the acid/base equilibrium for GPP is affected substantially by environmental  $\kappa$  (Figure S5 and Table S1), various polarity correction factors ( $\delta \sim 0.09$ – $0.13$  depending on different interface  $\kappa \sim 60.3$ – $63.0$ ) are considered to estimate interface pH and its deviation from the bulk pH ( $\Delta\text{pH}$ ) using eq. 5 and 6. Bulk pH and temperature-dependent interface pH and  $\Delta\text{pH}$  are listed in Table 1. A similar increase of  $\Delta\text{pH} \sim -0.5$  was mostly observed upon increasing temperature from 20 °C to 40 °C at bulk pH 4.9 and 4.4, respectively, although the major increase of  $\Delta\text{pH}$  was observed around the DMPG phase transition temperature (Figures 5 and 6, Table 1). As we observed that pH at typical self-assembly interface (SDS micelle) does not depend on temperature, the temperature dependent increase of Stern layer interface acidity for DMPG LUV should be associated with the DMPG gel to liquid-crystalline phase transition.

It has been reported that interface pH and  $\kappa$  for a charged amphiphilic self-assembled system are highly controlled by the packing arrangement of ionic headgroups at the interface Stern layer.<sup>9,27</sup> A tight headgroup packing arrangement with their low solvent accessible surface area restricts the electrostatic penetration of  $\text{H}_3\text{O}^+$  (for an anionic headgroup) or  $\text{OH}^-$  (for a cationic headgroup) and  $\text{H}_2\text{O}$  (for solvation) into the interface stern layer.<sup>9</sup> However, the penetrating ability are gradually improved with increasing inter-headgroup separation distance (loose headgroups packing) during gel to liquid-crystalline phase transition. The packing flexibility may allow the anionic headgroup to have more access to the bulk water phase for solvation and penetration of  $\text{H}_3\text{O}^+$  into the interface (Scheme 3).

**Scheme 3. Schematic representation of lipid headgroup packing arrangement in DMPG LUV in gel (left) and liquid-crystalline (right) phases.**



The higher  $\text{H}_3\text{O}^+$  penetration at the DMPG LUV interface makes the interface more acidic by  $\sim 0.5$  pH unit for liquid-crystalline phase compared to the gel phase. Notably, no significant change of pH at the SDS micelle interface was observed in the range of 20–40 °C (Table 1), which surely eliminates any role of intrinsic temperature induced pH change at LUV interface. On the other hand, only a small increase of interface  $\kappa$  from  $\sim 60$

to 63 was detected for the transition from gel to liquid-crystalline phase (inset of Figure 6 and Table 1). Presumably, the lipid phase transition-induced increase of interface  $\kappa$  may be partially compensated by increasing temperature-dependent decrease in  $\kappa$  (Table 1), resulting in the affection to the small change of interface  $\kappa$ .

## CONCLUSION

A series of UV-vis spectral changes shown by GPP (2) prove the utility of GPP (2) as a probe for the simultaneous evaluation of interface pH and polarity for amphiphilic self-assemblies. Throughout the UV-vis spectral changes during the protonation/deprotonation at inner nitrogen atoms in the porphyrin ring and aggregation character, GPP (2) is able to reflect the local pH and polarity in media around GPP (2). Furthermore, the delicately balanced structure composed of a porphyrin moiety (hydrophobic deprotonated or cationic protonated) and hydrophilic glucose parts in GPP (2) enable the compound to stay at the Stern layer of anionic phospholipid self-assemblies. The evaluation of physicochemical properties based on the spectral changes of GPP (2) in the presence of DMPG LUV is possible during the phase transition of the lipid self-assembly. The difference in  $\text{p}K_a$  between the bulk and the lipid membrane surface is interpretable in terms of structural dynamics of phospholipid self-assemblies that affects the interface ion penetration abilities. Designed chromophore probes, such as GPP (2), will be useful to understand chemical events on membrane surface.

## ASSOCIATED CONTENT

### Supporting Information

The Supporting Information is available free of charge on the ACS Publications website at DOI:XXXXXXXXXX.

Synthesis protocol and characterization for GPP(2), several UV-vis spectra, NOESY spectrum, DLS measurement results and a cryo-TEM image.

## AUTHOR INFORMATION

### Corresponding Author

\*tmatsuo@ms.naist.jp (T.M.)

\*parthaparui@yahoo.com (P.P.P.)

## ACKNOWLEDGMENT

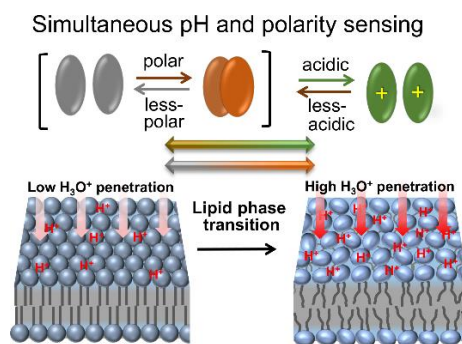
T. M. thanks a Grant-in Aid for Scientific Research on Innovative Areas “Molecular Engine” (JSPS KAKENHI Grant Number JP19H05395). S. N. also thanks a Grant-in Aid for Scientific Research (C) (JSPS KAKENHI Grant Number JP19K05695). PPP acknowledges UGC and government of West Bengal for financial support under RUSA 2.0 scheme (No: 5400-F(Y)). RM and SR acknowledges UGC for SRF fellowship. We thank Ms. Yoshiko Nishikawa for mass spectral analyses. We also acknowledge Prof. Shun Hirota for his kind help in usage of some experimental facilities.

## REFERENCES

- (1) Heimburg, T., *Thermal biophysics of membranes*. Wiley - VCH Verlag GmbH & Co. KGaA Weinheim, 2007.

- (2) Heimburg, T.; Jackson, A. D. On soliton propagation in biomembranes and nerves. *Proc. Natl. Acad. Sci. USA* **2005**, *102*, 9790–9795.
- (3) Ben-Dov, N.; Korenstein, R. Proton-induced endocytosis is dependent on cell membrane fluidity, lipid-phase order and the membrane resting potential. *Biochim. Biophys. Acta* **2013**, *1828*, 2672–2681.
- (4) Nambiar, R.; McConnell, R. E.; Tyska, M. J. Control of cell membrane tension by myosin-I. *Proc. Natl. Acad. Sci. USA* **2009**, *106*, 11972–11977.
- (5) Perez-Camacho, M. I.; Ruiz-Suarez, J. C. Propagation of a thermo-mechanical perturbation on a lipid membrane. *Soft Matter* **2017**, *13*, 6555–6561.
- (6) Freedman, S. D.; Kern, H. F.; Scheele, G. A. Acinar lumen pH regulates endocytosis, but not exocytosis, at the apical plasma membrane of pancreatic acinar cells. *Eur. J. Cell. Biol.* **1998**, *75*, 153–162.
- (7) Zhang, Z. S.; Nguyen, K. T.; Barrett, E. F.; David, G. Vesicular atpase inserted into the plasma membrane of motor terminals by exocytosis alkalizes cytosolic pH and facilitates endocytosis. *Neuron* **2010**, *68*, 1097–1108.
- (8) Neuhoff, S.; Ungell, A. L.; Zamora, I.; Artursson, P. pH-dependent passive and active transport of acidic drugs across caco-2 cell monolayers. *Eur. J. Pharm. Sci.* **2005**, *25*, 211–220.
- (9) Sarkar, Y.; Majumder, R.; Das, S.; Ray, A.; Parui, P. P. Detection of curvature-radius-dependent interfacial pH/polarity for amphiphilic self-assemblies: Positive versus negative curvature. *Langmuir* **2018**, *34*, 6271–6284.
- (10) Parui, P. P.; Sarkar, Y.; Majumder, R.; Das, S.; Yang, H.-X.; Yasuhara, K.; Hirota, S. Determination of proton concentration at cardiolipin-containing membrane interfaces and its relation with the peroxidase activity of cytochrome *c*. *Chem. Sci.* **2019**, *10*, 9140–9151.
- (11) Singh, M. K.; Shweta, H.; Khan, M. F.; Sen, S. New insight into probe-location dependent polarity and hydration at lipid/water interfaces: Comparison between gel- and fluid-phases of lipid bilayers. *PhysChemChemPhys* **2016**, *18*, 24185–2419.
- (12) Rudine, A. B.; DelFatti, B. D.; Wamser, C. C. Spectroscopy of protonated tetraphenylporphyrins with amino/carbomethoxy substituents: Hyperporphyrin effects and evidence for a monoprotated porphyrin. *J. Org. Chem.* **2013**, *78*, 6040–6049.
- (13) Liu, Y. Y.; Wu, M.; Zhu, L. N.; Feng, X. Z.; Kong, D. M. Colorimetric and fluorescent bimodal ratiometric probes for pH sensing of living cells. *Chem. Asian J.* **2015**, *10*, 1304–1310.
- (14) Villari, V.; Mineo, P.; Scamporrino, E.; Micali, N. Role of the hydrogen-bond in porphyrin *J*-aggregates. *RSC Adv.* **2012**, *2*, 12989–12998.
- (15) Verma, S.; Ghosh, A.; Das, A.; Ghosh, H. N. Ultrafast exciton dynamics of *J*- and *H*-aggregates of the porphyrin-catechol in aqueous solution. *J. Phys. Chem. B* **2010**, *114*, 8327–8334.
- (16) Meister, A.; Finger, S.; Hause, G.; Blume, A. Morphological changes of bacterial model membrane vesicles. *Eur. J. Lipid Sci. Tech.* **2014**, *116*, 1228–1233.
- (17) Akerlof, G. Dielectric constants of some organic solvent-water mixtures at various temperatures. *J. Am. Chem. Soc.* **1932**, *54*, 4125–4139.
- (18) Adler, A. D.; Longo, F. R.; Finarelli, J. D.; Goldmacher, J.; Assour, J.; Korsakoff, L. A simplified synthesis for meso-tetraphenylporphine. *J. Org. Chem.* **1967**, *32*, 476–476.
- (19) Lindsey, J. S.; Schreiman, I. C.; Hsu, H. C.; Kearney, P. C.; Marguerettaz, A. M. Rothmund and adler-longo reactions revisited - Synthesis of tetraphenylporphyrins under equilibrium conditions. *J. Org. Chem.* **1987**, *52*, 827–836.
- (20) Matile, S.; Berova, N.; Nakanishi, K.; Fleischhauer, J.; Woody, R. W. Structural studies by exciton coupled circular dichroism over a large distance: Porphyrin derivatives of steroids, dimeric steroids, and brevetoxin b. *J. Am. Chem. Soc.* **1996**, *118*, 5198–5206.
- (21) Maiti, N. C.; Mazumdar, S.; Periasamy, N. *J*- and *H*-aggregates of porphyrin-surfactant complexes: Time-resolved fluorescence and other spectroscopic studies. *J. Phys. Chem. B* **1998**, *102*, 1528–1538.
- (22) Riske, K. A.; Amaral, L. Q.; Lamy-Freund, M. T. Thermal transitions of dmpg bilayers in aqueous solution: SAXS structural studies. *Biochim. Biophys. Acta* **2001**, *1511*, 297–308.
- (23) Riske, K. A.; Fernandez, R. M.; Nascimento, O. R.; Bales, B. L.; Lamy-Freund, M. T. DMPG gel-fluid thermal transition monitored by a phospholipid spin labeled at the acyl chain end. *Chem. Phys. Lipids* **2003**, *124*, 69–80.
- (24) Cevc, G.; Watts, A.; Marsh, D. Titration of the phase-transition of phosphatidylserine bilayer-membranes - Effects of pH, surface electrostatics, ion binding, and headgroup hydration. *Biochemistry* **1981**, *20*, 4955–4965.
- (25) Lamy-Freund, M. T.; Riske, K. A. The peculiar thermo-structural behavior of the anionic lipid dmpg. *Chem. Phys. Lipids* **2003**, *122*, 19–32.
- (26) Watts, A.; Harlos, K.; Maschke, W.; Marsh, D. Control of the structure and fluidity of phosphatidylglycerol bilayers by ph titration. *Biochim. Biophys. Acta* **1978**, *510*, 63–74.
- (27) Nagarajan, R. Molecular packing parameter and surfactant self-assembly: The neglected role of the surfactant tail. *Langmuir* **2002**, *18*, 31–38.

## Graphical Abstract



1  
2  
3 A porphyrin-based probe for simultaneous detection of interface acidity and  
4 polarity during lipid phase transition of vesicle  
5  
6  
7  
8  
9  
10

11 Graphical Abstract

12  
13 Estimation of pH and polarity changes at an identical interface depth of membrane during gel to  
14 liquid-crystalline phase transition of lipid using a glucose-pendant porphyrin molecule.  
15  
16

